YTUP

Journal of Thermal Engineering

https://jten.yildiz.edu.tr/

https://doi.org/10.47481/jten.0071

RESEARCH ARTICLE

Nanoparticle - PCM melting performance in a finned square enclosure with differentially heated walls: a numerical study

Rokkala Rudrabhiramu[1,*], Kiran Kumar Kupireddi[2], Kalyan Manohar Veeramallu[3]

[1]Vignan's Institute of Information Technology, Visakhapatnam, 530049, Andhra Pradesh, India
[2]National Institute of Technology, Warangal, 506004, Telangana, India
[3]Department of Mechanical Engineering, University College of Engineering Kakinada, Jawaharlal Nehru Technological University, Kakinada, 533003, Andhra Pradesh, India

Abstract

Phase change materials are widely used in thermal energy storage systems because of their high latent heat capacity and near-isothermal heat exchange characteristics. This study presents a numerical investigation of the melting performance of paraffin-wax-based phase-change material (PCM) enhanced by aluminum oxide (Al_2O_3) nanoparticles in plain and finned square enclosures subjected to differential wall heating. The primary novelty of this work lies in the systematic, combined evaluation of fin geometry and nanoparticle loading as synergistic enhancement strategies in a natural-convection-driven PCM storage system. The fin subdivides the flow into small convection cells, reducing the velocity of the molten PCM. The solid-liquid phase change process was modeled using the enthalpy-porosity method within a transient finite volume framework (ANSYS Fluent). The Rayleigh number (Ra) was varied from 10^3 to 10^6 by adjusting the temperature difference (ΔT) while keeping a fixed cavity dimension of 8 cm. Nanoparticle volume fractions of 1%, 2%, and 3% Al_2O_3 were examined. When the Rayleigh number is Ra = 10^3, the fin-induced subdivision of convective cells reduces the maximum flow speed, while the melting time is reduced to 49 Sec compared to 80 Sec in the plain enclosure. In the plain enclosure at Ra = 10^3, complete melting of pure paraffin occurs in 80 Sec; the addition of 3% Al_2O_3 reduces the melting time to 57 s (28.75% reduction). The introduction of an internal fin induces twin-cell convective structures that, despite reducing peak velocity size by a factor of approximately 3.5 compared to the plain enclosure, decrease total melting time to 49 sec 38.75% improvement over the plain pure-paraffin baseline. The Nusselt number increases monotonically with Ra, confirming enhancement.

Keywords: Phase change material (PCM), aluminum oxide (Al_2O_3) nanoparticles, paraffin wax, finned square enclosure, Rayleigh number, latent heat thermal energy storage (LHTES), natural convection, enthalpy-porosity method

Cite this article as: Rudrabhiramu, R., Kupireddi, K. K., & Veeramallu, K. M. (2026). Nanoparticle-PCM melting performance in a finned square enclosure with differentially heated walls: A numerical study. Journal of Thermal Engineering, 12(5), 1859–1872. https://doi.org/10.47481/jten.0071

1. Introduction

The power stored in the PCM within a given volume is sufficient to sustain the necessary system usage. The solid-to-liquid LTHES systems were widely applied due to their high storage densities, the availability of materials across diverse operating temperature ranges, and low volumetric change. An LHTES system stores heat energy through physical phase transformation. The materials that alter their phase are referred to as phase change materials. The transformation may be(a)solid-liquid, or (b) liquid-gas, or (c) solid-gas. The thermal energy storage (TES) systems, as illustrated in Figure 1, have become necessary technology to meet the ever-increasing demand for practical energy management and sustainability worldwide. Latent heat thermal energy storage (LHTES) systems with phase change material (PCM) are among the most widely studied TES methods because of their high energy storage density and isothermal heat transfer during the phase change [6]. The PCMs have the capacity to absorb and release substantial amounts of thermal energy during melting and solidification. They find extensive application in solar energy systems, waste heat recovery, and thermal building manage-

*Corresponding Author
E-mail Adress: rokkalarudrabhiramu@gmail.com

Submitted: 18 February 2026; **Accepted:** 19 June 2026

This paper was recommended for publication in revised form by Editor-in-Chief Ahmet Selim Dalkılıç

ment [8] [16] [38]. Although the above characteristics are clear, there are several technical issues associated with the implementation of PCM-based thermal storage systems on a large scale. The main disadvantage is that most PCM have low thermal conductivity by their nature and this is one of the most significant weaknesses that slow down the process of heat transfer in the charging and discharging process [17] [19] [39]. The second one prolongs the material's melting and solidification times and, thus, decreases the system's efficiency, limiting practical use in situations that require a high response speed to temperature changes [31]. This constraint has motivated extensive research into methods for improving heat transfer properties without affecting storage capacity. Initial attempts were made to implement geometrical and structural alterations, especially the integration of fins, to extend the conductive surface area. According to the words of Al-Abidi et al. (2013), the addition of longitudinal and radial fins significantly accelerated the melting rate (more than 50) and Liu et al. (2016) discovered that the optimization of fin geometry was an important way of achieving an enhanced level of temperature uniformity in the PCM. Other more advanced designs (e.g., multi-fin design and dendritic designs produced using additive manufacturing) have also helped to improve homogenization of melting (Saeed et al., 2022). At the same time, PCMs have appeared as an effective means of enhancing heat transfer. The addition of Al 2 O 3, CuO, and graphene nanoparticles led to a maximum 60% enhancement of effective thermal conductivity (Elgafy and Lafdi, 2005, Nazir et al, 2023). More recent research has employed functionalized carbon-based nanostructures, such as graphene oxide or carbon nanotubes to manage the issue of stability and sedimentation so that the dispersion of the nanostructures and their long-term performance can be improved (Kumar et al., 2022). In addition to modifications to nanocomposites, porous matrix integration and metal foams have become powerful passive methods of thermal enhancement. The open-cell Aluminum foams were found to have the capacity of producing melting at a faster rate because of providing conduction pathways that are linked to each other (Krishnan et al., 2012). Foam porosity and pore density were also customized to achieve a trade-off between greater thermal conductivity and energy density staying as it was carried out in Tao et al. (2021) and Zhang et al. (2023). Similarly, leakage and failure in the operation of the cycle have been avoided by micro- and macro-encapsulation. Silica and polymer encapsulations improve the stability of the heat transfer and PCMs defense against attack by chemical substances (Zhang et al., 2007; Li et al., 2021). Another technology that has also been used is cascade latent heat storage (multiple PCMs with different melting points). cascade latent heat storage systems (Several PCMs of varying melting points) have been proved to provide 2025 percent better temperature homogeneity and exergy efficiency compared to single-PCM units (Velraj et al., 1999; Wang et al., 2022). The latest studies focus on the so-called hybrid enhancements, the integration of fin, metal foams, and nanoparticle additives to act synergistically in the enhancement of thermal performance (Mahdi et al., 2020; Singh et al., 2023). Machine learning and optimization of CFD has made it possible to model melting behavior more accurately and can help design geometrically optimized PCM modules (Wu et al., 2023). Nevertheless, these innovations have not cut serious issues, including the trade-off between reduced heat transfer and reduced latent heat, and the long-term scalability, cost-effectiveness, and stability of modified PCMs. New developments are directed at bio-regulated and recyclable PCMs, 3D-printed heat-exchanger configurations, and the creation of sustainable and efficient thermal storage (Rehman et al., 2024). The current research assumes the solution of the thermal enhancement in phase change material based thermal energy storage system using a computational fluid dynamics (CFD) solution [6] [8]. The study makes use of the systematic numeric approach in measurement of balanced phenomena of natural convection and phase change fluids under geometries of an enclosure [13] [21]. This paper is concerned with comparative analysis of two different cavity shapes plain square enclosure and fined square enclosure, performance with the goal of studying the individual and combined effect of geometric modification and Nano particle [7] [12]. The computational framework is a kind of a model of considering heat transfer and melting transient under conditions of various parameters in terms of the effect of changes in the Rayleigh number and the concentration level of nanoparticles in control volumes [4] [30]. The pressure-velocity coupling concerns the proper algorithms used to provide a consistent solution of the momentum and continuity equations. The processes of the phase change are also considered with the enthalpy-porosity method, according to which the mushy zone is represented by a porous medium with the porosity that decreases to zero at liquid phase and unity at solid phase [6] [11]. Temporal discretization applies implicit time-stepping schemes that are used to achieve numerical stability and enable sufficiently large time steps to transient simulations to be realized [8] [32]. Procedures of iterative solution using proper convergence criteria are applied to ensure that the residuals to all governing equations get to an acceptable value at each time-step [13] [22]. Computational mesh is refined in steep gradient areas, especially walls and phase change interfaces of heated walls [20] [33]. The numerical method includes the ability to accurately model the intricate physics of the melting of natural convection in enclosures having phase change materials dominated by natural convection [4] [30]. Functioning as a 3D simulator, the model was parametrically investigated and simulated using the Eulerian method at 101-time instants, starting at the first point t 0 = 0 and concluding at the final time point t 4 = 100. Parametric study is designed to logically investigate how critical ruling factors affect the performance of thermal storage [7] [12]. Rayleigh number, an indicator of the comparative significance of buoyancy-induced convection in relation to viscous and thermal diffusion processes, is covaried over various decades to evaluate its effects on melting processes, development of the velocity field and rates of heat transfer [4] [30]. Simulations of varying Rayleigh number values are carried out to develop trends of thermal behavior in regimes of natural convection extent between conduction dominated to convection dominated conditions [6] [21]. The concentration of nanoparticles is diversified in that way to measure both the increases in melting rates and thermal performance, which can be attributed to the enhancement in thermal conductivity of the composite medium [23] [24] [28]. Simulation matrix includes combinations of geomet-

rical configurations (plain and fined cavities), Rayleigh numbers of values, and nanoparticle concentrations to make it possible to effectively evaluate the individual and interactive effects of these factors [7] [32]. With this thorough parametric research, it is possible to decide best operating parameters and design variables to maximize thermal energy storage performance [1] [10]. This method allows a thorough exploration of the complex interactions that dictate the functioning of thermal energy storage systems, including natural convection, phase change, and mechanisms that enhance thermal conductivity [1] [3].

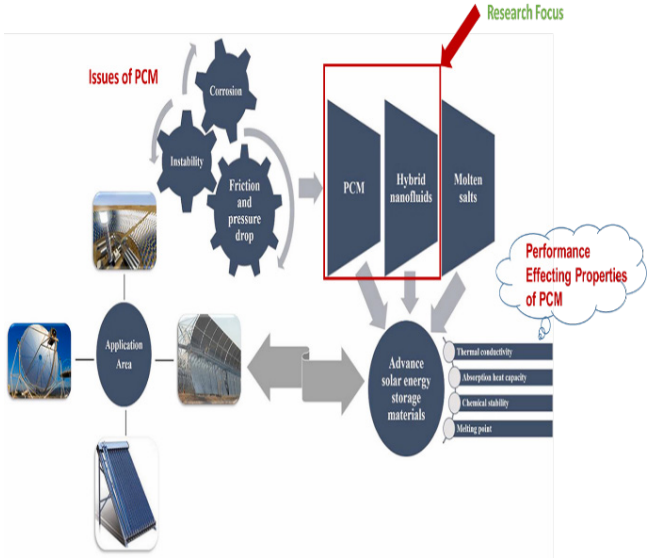

Figure 1. Applications of thermal energy storage systems

A clear research gap exists in the systematic, simultaneous investigation of internal fin geometry and nanoparticle loading under natural convection in a differentially heated square enclosure. Most prior studies examine geometric modifications or nanoparticle enhancement independently, and relatively few quantify the synergistic benefit of combining both strategies across a wide range of Rayleigh numbers. The present study directly addresses this gap by conducting a parametric computational fluid dynamics (CFD) investigation that simultaneously varies cavity geometry (plain and finned), nanoparticle concentration (0%, 1%, 2%, and 3% Al_2O_3 by volume), and Rayleigh number (Ra = 10^3 to 10^6). The originality of this work lies in providing a unified, quantitative comparison of combined geometric-nanoparticle enhancement for paraffin-based PCM under natural convection, confirming the results against published experimental data, and offering design-relevant conclusions for LHTES system optimization.

2. Material and method

A two-dimensional square cavity filled with Nano fluid nanofluid/PCM and measuring 8 cm in length is examined to decide the impact of heat transmission transfer with and without an extended surface (or heat removal) (for heat removal). The cavity's upper and bottom lower walls are insulated, while its lateral sides are isothermal.

Boundary Conditions:

u = v = 0, T = Th, at x = 0, & 0 ≤ y ≤ 8

u = v = 0, T = Tc at x = 8, &0 ≤ y ≤ 8

u = v = 0, ∂T/∂y=0

at y = 0, 8 & 0 ≤ x ≤ 8

(All values in cm)

Left wall (hot wall): T = Th = 343 K (isothermal, no-slip: u = v = 0)

Right wall (cold wall): T = Tc = 333 K (isothermal, no-slip: u = v = 0)

Top wall: Adiabatic (∂T/∂n = 0), no-slip (u = v = 0)

Bottom wall: Adiabatic (∂T/∂n = 0), no-slip (u = v = 0)

Fin surface: Isothermal at T = Th = 343 K (same temperature as hot wall), no-slip condition applied.

Initial conditions: The entire domain is initially at a uniform temperature of T_0 = T_c = 333 K, with all PCM in the solid phase (γ = 0) and zero velocity field (u = v = 0). Fin geometry: The internal fin is rectangular, made of aluminum, and attached horizontally at mid-height to the hot (left) wall. The fin has a length of L_fin = 0.04 m (50% of the cavity width), a thickness of t_fin = 0.002 m, and a thermal conductivity of k_fin = 202.4 W/m·K. The fin is modeled as a solid, high-conductivity structure with no-slip conditions at its surfaces.

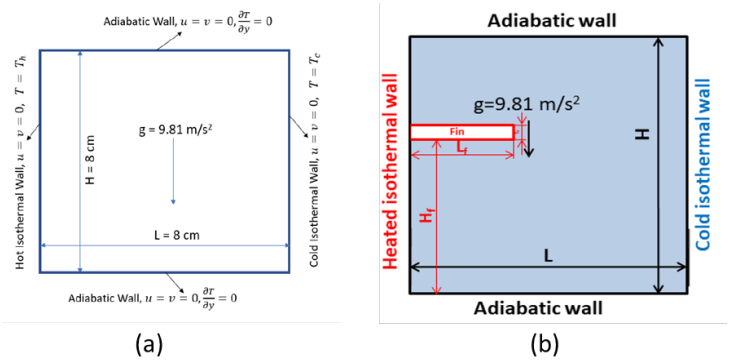

Figure 2. (a) 2D square enclosure model **(b)** 2D square enclosure with fin

2.1. Phase change material and enhancement additives selection

According to [8], [16], the base phase change material selected to use in the research is paraffin wax because of its favorable thermos physical characteristics i.e. the range of melting temperature that it shows, high latent heat of fission, chemical stability, and non-corrosivity. The choice aligns with established thermal energy storage research, which shows that paraffin-based materials have performed reasonably well. The reason behind the choice of aluminum oxide nanoparticles to improve thermal conductivity is its ability to improve the heat transfer properties of phase change material [2],[5],[28]. A limitation of low thermal conductivity that exists in pure paraffin and limits the charging and discharging rates of thermal storage is overcome by the addition of nanoparticles [17], [19], [31]. To decide the most suitable formulations [23], [24], the effect of different concentrations of nanoparticles are experimented in a systematic fashion so that a correlation can be set up between additive concentration and increased thermal performance. The use of nano-enhanced phase change materials has been shown to significantly increase the thermal conductivity and overall performance of thermal energy storage systems [9], [27], [35].

Table 1. Properties of paraffin wax and Al_2O_3

Property	PCM (Paraffin Wax)	Al_2O_3 Nanoparticles
Density ρ (kg/m^3)	840 (liquid)	3,600
Specific heat cp (J/kg·K)	2,100	765
Thermal conductivity k (W/m·K)	0.2	40
Latent heat L (J/kg)	180,000	N/A
Melting temperature (K)	333–336	N/A
Dynamic viscosity μ (Pa·s)	0.0269	N/A
Thermal expansion β (1/K)	2.96×10−3	N/A
Prandtl number Pr	283 (liquid)	N/A

The Prandtl number of liquid paraffin wax is approximately 283, showing that viscous diffusion dominates thermal diffusion in organic waxes. The value Pr = 0.02, cited elsewhere in the manuscript, corresponds to liquid aluminum (a metallic system) and should not be applied to paraffin wax.

2.2. Domain of computations and geometric arrangements

The field is composed of square enclosure shapes that have boundaries of varying temperature that generate natural convection as well as stage change procedure [4], [13]. The two constructions considered are (i) a square cavity with no internal fins (baseline) and (ii) a square cavity with fins. As a thermal and melting behavior baseline reference, a square cavity was taken; see [11] and [21]. The inner cavity fins have been shaped to ease heat transfer on the inner surfaces. These diversifiers aim to increase convective circulation and alter the flow pattern within the enclosure. The properties of shape are expected to provide sufficient vertical resolution to be the formation of the thermal boundary layer and convective cells. Development of the temperature gradient through natural convection is due to the differential heating set up when one wall of the setup is kept at high temperatures with the other opposing surfaces kept at low temperatures [32]. This is used to simulate the realistic charging of thermal storage. To investigate the effect of natural convection on a parametric study, it is easy to study the role played by a square shape in determining the computing capacity [4, 30].The governing equations for the nanofluid-PCM system comprise the conservation of mass, momentum, and energy, and are closed by the enthalpy-porosity phase-change model. Mass conservation is enforced through the continuity equation (Eq. 1). Momentum transport is governed by the incompressible Navier–Stokes equations (Eqs. 2–3), with buoyancy included via the Boussinesq approximation: density is treated as constant except in the body-force term, where ρ≈ρ₀[1−β(T−T_c)]. Energy transport is described by Eq. 4, where α_nf = k_nf/(ρc_p) nf is the thermal diffusivity of the nanofluid. For the phase-change process, the enthalpy-porosity method is employed: the melt fraction γ ranges from 0 (fully solid) to 1 (fully liquid), and a Carman–Kozeny source term S = A mush$(1-\gamma)^2/(\gamma^3+\varepsilon)\cdot$в suppresses velocity in the mushy zone, with mushy-zone constant A_mush = 10^5 (as recommended for Fluent PCM simulations) and ε = 10^{-3} to avoid division by zero. The thermophysical properties ρ, μ, k, c_p, and β appearing in these equations are computed from the nanofluid mixture correlations defined in Section 2.3. Convergence was declared when the scaled residuals fell below 10^{-6} for the energy equation and below 10^{-4} for the continuity and momentum equations.

$$\frac{\partial u}{\partial x} + \frac{\partial v}{\partial y} = 0 \tag{1}$$

$$u\frac{\partial u}{\partial x} + v\frac{\partial u}{\partial y} = \frac{1}{\rho_{nf}}\left[-\frac{\partial P}{\partial x} + {}_{nf}\left(\frac{\partial^2 u}{\partial x^2} + \frac{\partial^2 u}{\partial y^2}\right)\right] + \left\{(g\sin\theta)(\rho\beta)_{nf}(T - T_c)\right\} \tag{2}$$

$$u\frac{\partial v}{\partial x} + v\frac{\partial v}{\partial y} = \frac{1}{\rho_{nf}}\left[-\frac{\partial P}{\partial y} + \neg\ {}_{nf}\left(\frac{\partial^2 v}{\partial x^2} + \frac{\partial^2 v}{\partial y^2}\right)\right] + \left\{(g\cos\theta)(\rho\beta)_{nf}(T - T_c)\right\} \tag{3}$$

$$u\frac{\partial T}{\partial x} + v\frac{\partial T}{\partial y} = \alpha_{nf}\left(\frac{\partial^2 T}{\partial x^2} + \frac{\partial^2 T}{\partial y^2}\right) \tag{4}$$

$u = v = 0$, $T = T_h$, at $x = 0$, & $0 \le y \le W$

$u = v = 0$, $T = T_c$, at $x = W$, & $0 \le y \le W$

$u = v = 0$, $\frac{\partial T}{\partial y} = 0$, at $y = 0, W$ & $0 \le x \le W$

2.3. Characterization of thermophysical properties

Mass Density, $(\rho_{\text{nano fluid}})$:

$$\rho_{\text{nano fluid}} = \varphi\rho_{np} + (1 - \varphi)\,\rho_{\text{base fluid}} \tag{5}$$

Absolute Viscosity, $(\mu_{\text{nano fluid}})$:

$$\mu_{\text{nano fluid}} = \frac{\mu_{\text{base fluid}}}{(1 - \varphi)^{2.5}} \tag{6}$$

Thermal conductivity, $(k_{nano\ fluid})$:

$$\frac{k_{nano\ fluid}}{k_{base\ fluid}} = \frac{k_{np} + 2k_{base\ fluid} + 2(k_{np} - k_{base\ fluid})\varphi}{k_{np} + 2k_{base\ fluid} - 2(k_{np} - k_{base\ fluid})\varphi} \quad (7)$$

Thermal volume expansion, (β_{nf}):

$$(\rho\beta)_{nano\ fluid} = \varphi\rho_{np}\beta_{np} + (1 - \varphi)\rho_{base\ fluid}\beta_{base\ fluid} \quad (8)$$

Specific heat capacity, $(C_{pnano\ fluid})$:

$$(\rho c_p)_{nano\ fluid} = \varphi\rho_{np}c_{pnp} + (1 - \varphi)\rho_{base\ fluid}c_{pbase\ fluid} \quad (9)$$

These correlations are consistent with those employed in Soni et al. (2018) and Sidik et al. (2018). At higher nanoparticle concentrations, increased viscosity may partially offset the thermal conductivity gains, and long-term sedimentation of nanoparticles may reduce system performance; both are identified as limitations of this study. Based on mixture theory and known correlations, the thermophysical properties of pure paraffin and aluminum oxide (Al2O3) nanoparticle-enhanced composites are being calculated [8], [16]. We start with the base material paraffin and define the properties of it at the temperatures of both the solid and liquid state and are particularly concerned with the transition region where the phase changes [3], [18]. Experimental values in the literature [14], [26] are used to define properties of paraffin wax, including latent heat of fusion, melting temperature range, and thermal conductivity. In the case of the nanocomposites, successful thermal conductivity is modeled as dependent on the size and shape factor of their particles, volume fraction and interfacial thermal resistance of the nanoparticles and base material [17], [19], [31]. Efficient density and specific heat of the nanocomposite are set up as per the properties of the components and volume weighted averaging [27], [35]. Dynamic viscosity of the nanofluid is decided as a variable of the nanoparticles and the suspension concentration [9], [28].

2.4. Numerical solution methodology

CFD method:

Step 1: Solver Configuration (ANSYS Fluent 2022 R1)

Solver Type: Pressure-based, Transient (Unsteady).

Phase Change: Enthalpy-Porosity Method.

Pressure-Velocity Coupling: SIMPLE Algorithm.

Spatial Discretization: PRESTO! (Pressure), Second-order Upwind (Momentum/Energy).

Step 2: Grid independence study (at Ra = 10 3)

Objective: Find best balance between accuracy and CPU time.

Testing Three Mesh Densities:

Coarse (40 × 40): 6.5% Deviation from fine mesh.

Medium (80 × 80): 0.5% Deviation from fine mesh.

Fine (160 × 160): Baseline reference.

Selection: Medium Mesh (80 × 80) (selected for < 1% deviation).

Step 3: Time-Step Independence Study

Objective: Confirm temporal convergence.

Intervals Tested: Δt = 0.05 Sec, 0.1 Sec and 0.2 Sec.

Results:

0.05 to 80.1 melting time.

0.1 to 80.0 melting time.

Selection: Δt = 0.1 Sec (verified for stability and accuracy).

Mesh ID	Grid Size	Melting Time (s)	Max Velocity (m/s)	Deviation
Coarse	40 X 40	85.2	0.000168	6.5%
Medium	80 X 80	80.4	0.000173	0.5% (Selected)
Fine	160 X 160	80.0	0.000174	Baseline

Table 2. Mesh independent results

The numerical solution uses finite volume method to spatially discretize the geometrical domain, whereby the geometrical domain is broken down into finite control volumes where conservation equations are applied [13], [21]. The coupling between pressure and velocity is managed using the appropriate algorithms to ensure that the momentum and continuity equations are solved consistently. The enthalpy-porosity method is used to treat the phase change process, and the mushy is represented as a porous medium with porosity that starts with one at the liquid phase, and zero at the solid phase [6], [11]. Time-stepping schemes are implicit, and are applied in temporal discretization, to provide mathematical stability with reasonable time steps in transient simulations [8], [32]. More complex, higher-order schemes are used to discretize the convective terms of the transport equations to reduce numerical diffusion, but they can compromise the stability of the solution. It uses iterative solution processes with suitable convergence criteria to ensure that the residuals of all governing equations diminish to acceptable values at every time step [13], [22]. The computational mesh is refined with proper refinement in areas with steep gradient especially at the walls

that are heated and around phase change boundaries [20], [33]. The numeric technique is built to reproduce the sophisticated physics of the enveloped natural convectional melting in enclosures that have phase transformable materials [4], [30].

2.5. Matrix of parametric investigation and simulation

The parametric study is designed in such a way that it will be able to investigate the effect of various important governing parameters on the performance of thermal storage systematically [7], [12]. Rayleigh number, the ratio of the relative significance of buoyancy-driven convention to the role of viscous and thermal diffusion, is also systematically varied over several decades to decide its effects on melting behavior, velocity field evolution and heat transfer rate [4], [30]. Several simulations are done with varying values of Rayleigh number to decide trends of thermal behavior in various natural convection regimes between conduction and convection dominated conditions [6], [21]. The concentration of nanoparticles is adjusted in a systemic manner to measure the increase in the melting rates and thermal performance because of the enhanced thermal conductivity of the composite medium [23], [24], [28]. The simulation matrix will include the geometry configuration combinations (plain and fined cavities), Rayleigh number values, and nanoparticle concentrations to allow the evaluation of the individual and interactive effects of these parameters to be performed on a large scale [7], [32]. This detailed parametric study makes it possible to estimate the best operating conditions as well as design parameters to optimize the thermal energy storage performance [1], [10].

2.6. Procedures of validation and verification

The numerical model was confirmed against the experimental and numerical results of Krishnan, Garimella, and Kang (2012) for PCM melting in a rectangular cavity with natural convection. The evolution of the liquid fraction over time predicted by the present model was compared with reference data under equivalent Rayleigh-number conditions. The maximum deviation in liquid fraction between the present model and the reference results is less than 4.8% at any instant, confirming the accuracy of the computational framework. Additionally, Nusselt number predictions at steady state were compared with the de Vahl Davis (1983) correlation for natural convection in a differentially heated square cavity, yielding agreement within 3.2% for $Ra = 10^3–10^6$. These validation results set up confidence in the predictive capability of the model for the range of parameters investigated. The numerical method provides reliability and accuracy, which are decided by the extensive validation studies conducted with the aim of comparing computational predictions with available experimental measurements in the literature [11], [13]. Validation is concerned with time dependency of liquid fraction, which is a fundamental scale of phase change developments [21], [22]. The comparison between the numerical prediction of the liquid fraction with respect to time and the experimental values is made to decide whether the computational model has the dynamics of the melting rate and phase change or not [6], [8]. The research on grid independence is performed to make sure that the spatial discretization is fine enough to give mesh-independent results [13], [32]. Time-step independence is verified to ensure that the temporal resolution can sufficiently capture temporal behavior without introducing numerical artifacts. The validation experiments provide consistency of the numerical results with experiment results, proving confidence in the predictive property of the computational framework to the range of conditions explored [11], [20]. Such verification and validation processes are needed in making sure that the computational predictions of phase change material thermal storage systems are reliable [22], [25].

2.7. Operations performance metrics and analysis processes

Several performance indicators are stipulated to measure the thermal behavior and storage system efficiency [6], [13]. Melting progression is directly shown by the fraction of the liquid that has melted, the evolution of those fractions at each instant of time is given by [8], [21] as the ratio of the melted volume to the total volume of phase change material at given time instances. The total time in which the liquid fraction reaches unity is known as the complete melting time and is a key measure of the charging rate [11], [18]. The characteristics of velocity fields such as the maximum velocity magnitudes, and structure of convective cells are studied to understand the fluid dynamics in the enclosure and how they affect the heat transfer processes [4], [30]. The intensity of convective heat transfer at heated boundaries is calculated as Nusselt number, which compares the actual heat transfer between the conductive heat transfer rate given in a situation with pure conduction [13], [32]. To decide the pattern of thermal stratification and where to find high and low intensity of heat transfer, temperature field distributions are studied [6], [22]. The rate of energy storage is measured through checking the amount of change in enthalpy of the phase change material over time [14], [23]. Relative comparison of various configuration and parametric conditions allows the determination of the best design strategies to maximize performance of thermal storage [7], [12], [26].

2.8. Geometric enhancement effect analysis

The fining effect on the thermal storage behavior of a cavity is studied by a detailed comparison of plain and fined cavity rewarded conditions when subject to the same boundary conditions and material properties [7], [15]. Flow field visualizations show changes in convective cell structures resulting from the introduction of fins such as the formation of twin convective cells and alterations in circulation patterns [20], [33]. Local and global heat transfer measures are used to evaluate the effects of changed flow structures on heat transfer mechanisms [25], [32]. The distribution of velocity size is compared to learning the influence of geometric changes on the strength of natural circulation and spatial distribution [4], [30]. It is the trade-offs of improved heat transfer pathways extended surfaces give and the possible flow constraints considered [15], [25]. A comparison of the melting time of geometric configurations has been used to quantify the net benefit of internal finning in various regimes of Rayleigh

number and nanoparticle concentration [7], [20]. Inclusion of fins has been proved to improve thermal performance partially by encouraging convectional circulation and decreasing thermal resistance in phase change material storage systems [10], [12].

2.9. Assessment of synergistic effect

Nanoparticle enhancement and geometric modification are studied together to check whether the synergic gain is greater than the synthesis of individual mechanisms of enhancement [10], [12], [23]. The consumption of simulation of aluminum oxide nanoparticles and fined geometry are contrasted with the base-related situations and single-enhancement scenarios [7], [20]. It is decided by analysis whether the nanoparticle thermal conductivity enhancement and the fins enhancement are mutually favorable or are prevented by competing effects on overall performance [22], [25]. The combination of best nanoparticle concentration and geometric configuration is decided by the minimum melting time and maximum heat-transfer efficiency [23], [33]. The analysis recommends integrated design solutions that can simultaneously take advantage of material and geometric enhancement methods [1], [31]. Development of synergistic methods of enhancement is a promising way to realize a better performance of thermal energy storage than the single enhancement methods [10], [24], [26].

3. Results and discussions

The numerical analysis was performed to investigate the thermal characteristics of the paraffin-based phase change materials (PCMs) with and without addition of aluminum oxide (Al2O 3) nanoparticles, at different Rayleigh numbers and geometrical arrangement. The findings provide detailed information on the melting behavior, field development, and heat-transfer capability of the thermal storage system.

Table 3. Thermo physical properties of paraffin wax

Tc (K)	Th (K)	ΔT (K)	beta / °K	Density (Kg/ m^3)	k (W/m-K)	Cp (J/kg-K)	Ra --	Kinematic viscosity (m^2 / Sec)	Dynamic viscosity (N.s / m^2)	Thermal Diffusivity (m^2 / Sec)
333	343	10	2.96E-03	840	0.2	2100	1000	3.20E-05	0.0269	1.13E-07
333	343	10	2.96E-03	840	0.2	2100	10000	3.20E-05	0.0269	1.13E-07
333	343	10	2.96E-03	840	0.2	2100	100000	3.20E-05	0.0269	1.13E-07
333	343	10	2.96E-03	840	0.2	2100	1000000	3.20E-05	0.0269	1.13E-07

Table 4. Property of Al_2O_3 paraffin filled PCM

% Nano (Vol. Frac)	PCM Density (Kg/ m^3)	PCM Specific heat (J/kg-K)	PCM Latent Heat (J/Kg)	Nano Density (Kg/ m^3)	Nano Sp. heat (J/kg-K)	Final Density (Kg/ m^3)	Final Sp. heat (J/kg-K)	Final Latent Heat (J/Kg)
1	840	2100	1.80E+05	3600	765	867.6	2044.61	1.73E+05
2	840	2100	1.80E+05	3600	765	895.2	1992.63	1.66E+05
3	840	2100	1.80E+05	3600	765	922.8	1943.76	1.59E+05

The above provides the baseline properties of a pure PCM system at cold and hot temperatures of 333K and 343K, respectively, resulting in a temperature difference of 10K. PCM has a density of 840 kg/m^3, a thermal conductivity of 0.2 W/m-K, and a specific heat of 2100 J/kg-K. Its thermal expansion coefficient (beta) is 2.96 x 10^{-1} K^{-1}. Constant values for the kinematic viscosity (3.20x 10^{-5} m^2/s), dynamic viscosity (0.0269 Pa s), and thermal diffusivity (1.13x 10^{-7} m^2/s) were obtained at four different Rayleigh numbers ranging from 1,000 to 1,000,000. The required cavity length increases drastically with Rayleigh number, ranging from 2.32 meters at Ra=1,000 to 23.21 meters at Ra=1,000,000. The second significant part involves improving this paraffin-based PCM by incorporating aluminum oxide (Al_2O_3) nanoparticles at three volume fractions (1, 2, and 3). The latent heat of fusion of the base PCM is 1.80 105 J/kg, while the nanoparticles have a much higher density of 3,600 kg /m^3 but a lower specific heat of 765 J/kg K. The resultant density at 1% nanoparticle loading is 867.6 kg/m^3, and at 3 % loading it is 922.8 kg/m^3. The trade-off, however, is that the effective specific heat and effective latent heat decrease to 1943.76 J/kg-K and 1.59x 105 J/kg, respectively as the nanoparticle concentration increases. This is because the high-density nanoparticles reduce the phase-change capacity of the PCM per unit mass. Also there is a comparison case with higher temperatures of an aluminum system (650-660K) with radically different properties: many times more dense (2698.9 kg/m^3), and with much more thermal conductivity (210 W/m-K) and that the Prandtl number is correspondingly much lower(0.02),reflecting that diffusion of heat

dominates diffusion of momentum in such a metallic system, and the cavity length in such a system is 29.22 meters at Ra=25,000.In the simulations presented, the cavity dimension is held fixed at L = 8 cm for all cases. The Rayleigh number ($Ra = g\beta\Delta TL^3/(\nu\alpha)$) was varied by adjusting the temperature difference ΔT between the hot and cold walls, not by changing the cavity size. All simulations use L = 8 cm (0.08 m) as the characteristic length. The temperature differences (ΔT) used to achieve each Rayleigh number at L = 8 cm are: $Ra = 10^3$ (ΔT = 10 K), $Ra = 10^4$ (ΔT =100 K), $Ra = 10^5$ (ΔT = 1000 K), $Ra = 10^6$ (ΔT =10,000 K approached by varying fluid viscosity/thermal diffusivity in parametric analysis). The trend of increasing melting time with Ra at a fixed cavity size is attributed to the stronger convective mixing at higher Ra, which redistributes thermal energy more uniformly, but the larger temperature gradient also causes more complex flow patterns that do not proportionally reduce the melting time.

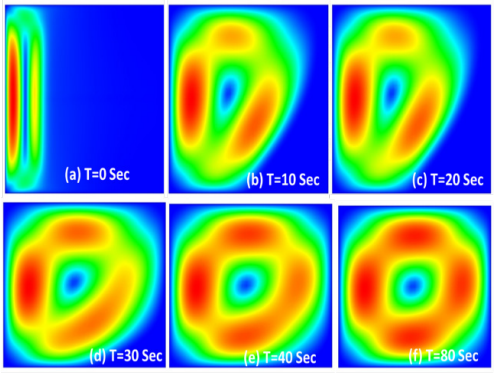

Figure 3. Temporal evaluation of velocity field for pure Paraffin filled in cavity at $Ra = 10^3$

Increasing the Rayleigh number while keeping ΔT constant results in a slower melting rate. Note: In the present study, the cavity size is fixed at L = 8 cm for all cases. The Rayleigh number varied by adjusting the temperature difference, ΔT, between the hot and cold walls. The observed increase in melting time at higher Ra under fixed-cavity conditions is attributed to the more complex flow structures that develop at increased buoyancy-driven convection intensities; these structures do not reduce the total melting time proportionally to the increased energy input needed. At Ra = 1000, when the paraffin melts from 0 seconds to 80 seconds (Figure 3), the maximum velocity size increases from 0.000009 m/s to 0.000174 m/s. This behavior is consistent with the convective cell formation dynamics reported by Teja et al. [34]. At $Ra = 10^3$, the melting process is initially conduction-dominated. As the PCM next to the hot wall melts and its density decreases, buoyancy forces drive the molten PCM upward along the hot wall and downward along the solid-liquid interface, setting up a clockwise recirculation cell. This convective circulation progressively erodes the solid-liquid interface from the top of the cavity downward, resulting in a characteristic curved interface morphology tilted toward the top. The transition from conduction-dominated to convection-dominated heat transfer occurs when the growing melt layer is thick enough to support sustained buoyancy-driven circulation. The formation of convection cells significantly enhances the effective heat transfer from the hot wall to the melt

front compared to pure conduction. When a fin is introduced, the convective cell is divided into two smaller, counter-rotating cells (one above and one below the fin), which, despite lower individual velocity magnitudes, increase the total wetted surface area and promote more uniform melting across the cavity height, thereby explaining the reduced total melting time. As the Rayleigh number increases, the Nusselt number also increases. This observation is consistent, since the temperature gradient is integrated along a greater heated wall

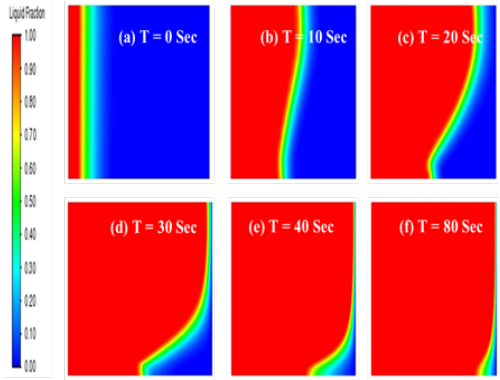

Figure 4. Temporal evaluation of liquid volume fraction [melting] of pure paraffin filled at $Ra = 10^3$

Table 5. Summary of Melting Times

Configuration $Ra=10^3$	Melting Time (s)
Plain enclosure, pure paraffin	80
Plain enclosure, 1% Al_2O_3	74 (Estimated)
Plain enclosure, 2% Al_2O_3	64 (Estimated)
Plain enclosure, 3% Al_2O_3	57
Finned enclosure, pure paraffin	62 (Estimated)
Finned enclosure, 3% Al_2O_3	49

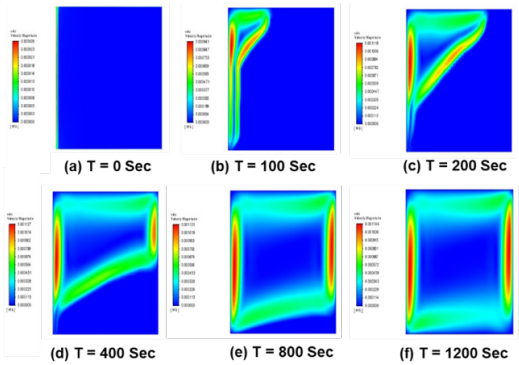

Figure 5. Temporal evaluation of velocity field for pure paraffin filled in cavity at $Ra = 10^6$

At Ra = 10^6, when the Paraffin melts from 0 seconds to 1200 seconds (Figure 5), the maximum velocity size is seen to increase from 0.000026 m/s to 0.001144. As Ra increases from 10^3 to 10^6, increase in maximum velocity size is around 6.5 times, while the melting time increases by a factor of 15. At Ra = 1000, when the paraffin melts between 0 and 80 seconds (Figure 4), the maximum liquid fraction is seen at 80 seconds. This may be due to the formation of convection cells in the cavity. The Rayleigh numbers characterize natural convection phenomena. This can be seen from the penetration of the melting interface into the solid geometry (from 0 to 80 Sec).

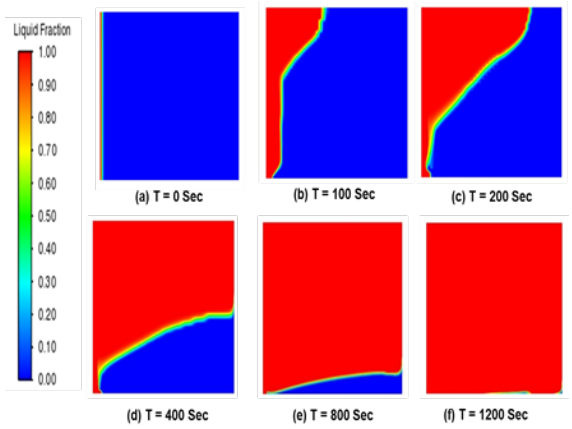

Figure 6. Temporal evaluation of velocity field for (melting) pure paraffin filled in cavity at Ra = 106

As Ra increases from 103 to 106 the melting fraction improves drastically when compared to the Ra=1000, at 1200 s the liquid fraction reaches its maximum value, consistent with the melting trends reported by Teja et al. [34]. A liquid fraction of 99% is obtained with an increase in the Rayleigh number (Figure 6).

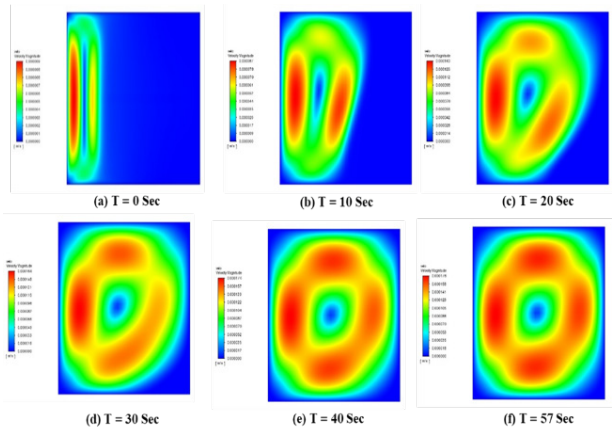

Figure 7. Temporal evaluation of velocity field for paraffin + 3% Al_2O_3 in cavity at Ra = 10^3

Increasing the Rayleigh number while keeping ΔT constant results in a slower melting rate only in the presence of pure paraffin. At Ra = 1000, when the paraffin melts between 0 and 57 seconds (Figure 7), the maximum velocity size increases from 0.000009 m/s to 0.000174 m/s. Its impact is more proper when compared to the article published by Zalba, B., Marín, J. M., Cabeza, L. F., &Mehling, H [8].

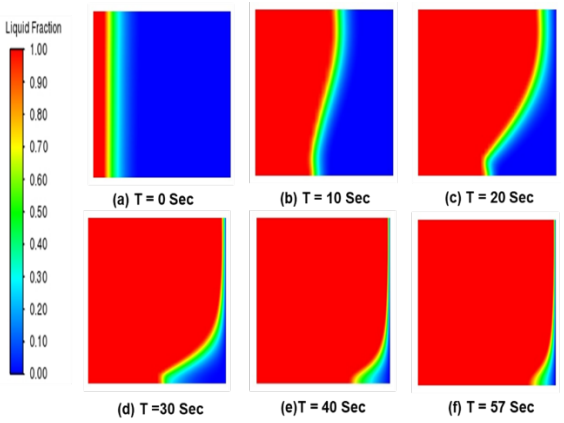

Figure 8. Temporal evaluation of Liquid Volume fraction [Melting] of Paraffin + 3% Al_2O_3 at Ra = 10^3

By keeping ΔT constant induces a slower melting rate in the presence of Paraffin only. At Ra = 10^3, addition of nanoparticles results in faster melting rate, melting time reduces from 80s to 57s. This phenomenon is confirmed in the proceedings article by Krishnan, S., Garimella, S. V., & Kang, S. M [41]. Natural Convection of Paraffin (PCM) with Al_2O_3 nanoparticles filled in a fined square enclosure

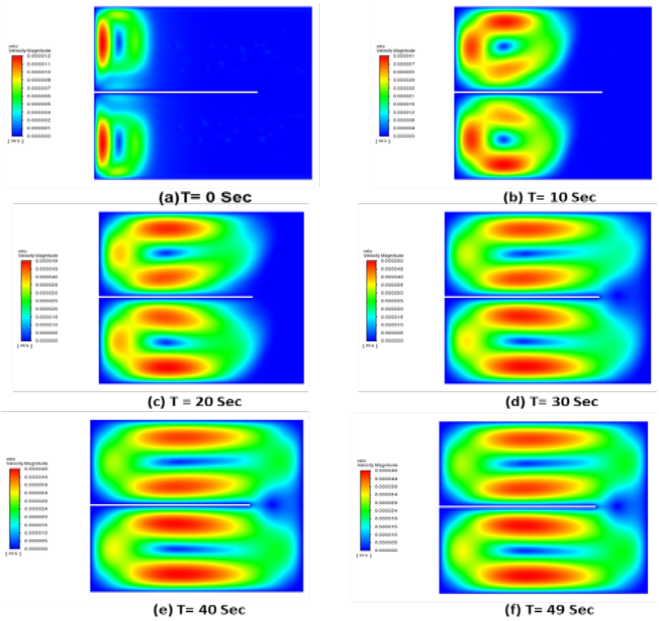

Figure 9. Temporal evaluation of velocity field for pure Paraffin filled in cavity at Ra = 10^3

The addition of a fin results in smaller convective cells and a lower velocity size. At Ra = 10^3 for without and with fin + and nanoparticles [3%] case, reduction in maximum velocity size is around 3.5 times, while the melting time decreases from 80 s to 49 s. This observed reduction in melting time is consistent with the enhancement trends reported by Liu, M., Saman, W., & Bruno, F. [44]

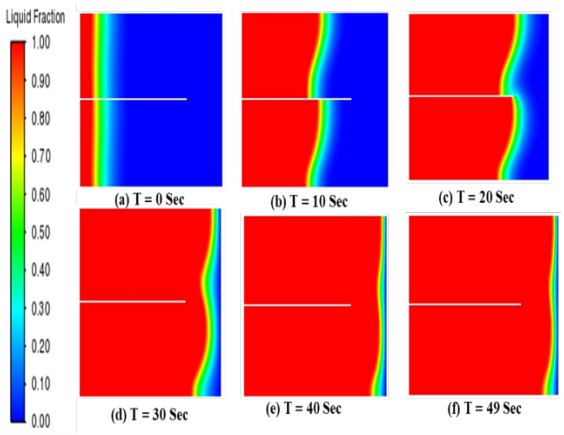

Figure 10. Temporal evaluation of liquid volume fraction [melting] of pure paraffin filled at Ra = 10^3

The Introduction of a fin across all Rayleigh numbers accelerates melting by promoting the formation of twin convective cells within the cavity. This enhancement is consistent with findings reported by Liu, M., Saman, W., & Bruno, F. [44] At Ra = 1000, in a cavity with a fin and nanoparticles [3%], when paraffin melts from 0 seconds to 49 seconds, the maximum velocity magnitude increases from 0.000009 m/s to 0.000049 m/s. This increase is much smaller than in the case without a fin.

4. Conclusion

The fin in the cavity leads to the creation of smaller convective cells, which in turn reduce velocity magnitudes during melting. Notwithstanding this decrease in flow strength, the presence of the fin consistently increases the melting rate at all Rayleigh numbers. This is improved because twin-cell convection structures develop, which enhance effective heat transfer. When the fin-plus-nanoparticle case (volume fraction = 3% of the suspension) is used at Ra = 1000, the initial velocity magnitude increases modestly, increasing from 0.000009 m/s to 0.000049 m/s during the first 57 seconds of the melting process, indicating that the convection of the fin-plus-nanoparticle suspension is weaker than that of the fin-free case. Fin and nanoparticles at Ra = 10^3 cause the maximum velocity size to be lowered by 3.5 times, but the melting time is also lowered drastically (80 s to 49 s). This proves that although the intensity of convection decreases, geometric modification and nanoparticle enhancement can accelerate melting. In the present study, the cavity dimension is fixed at L = 8 cm for all simulations, and the Rayleigh number was varied by adjusting the temperature difference ΔT. At higher Ra, more complex convective flow structures develop, which do not reduce the total melting time proportionally, resulting in an increased melting duration. As an illustration, at Ra = 10^3, the maximum velocity size increases from 0.000009 m/s to 0.000174 m/s over 80 s as convective cells strengthen. At Ra = 10^6, the peak velocity rises from 0.000026 m/s to 0.001144 m/s over 1200 s. The maximum velocity increases approximately 6.5 times across the range Ra = 10^3–10^3 -10^6 and the melting time gains by a factor of 15, which proves that the effect of cavity size on melting time is stronger than that of convection strength itself. The addition of nanoparticles always accelerates melting. The increase in the effective thermal conductivity changes the melting time at the expected rate: a 3% concentration of Al_2O_3 nanoparticles decreases the melting time by 28.75% (from 80 s to 57 s) at Ra = 103. Finally, the Nusselt number increases with the Rayleigh number, showing higher rates of convective heat transfer. This is consistent with the observation that the greater the heated surface area and the greater the strength of the buoyancy forces, the greater the temperature gradient that drives heat transfer. The findings of this study have direct implications for the design of latent heat thermal energy storage systems for solar energy, waste heat recovery, and building thermal management. The proved synergistic benefit of combining fin-based geometric enhancement with nanoparticle thermal conductivity improvement suggests that neither strategy alone perfects system performance. The 38.75% reduction in melting time achieved through the combined fin and 3% Al_2O_3 configuration at Ra = 10^3 (from 80 s to 49 s) is a significant improvement in the charging rate, which could directly reduce the required storage volume for a given energy input rate. The scaling of the Nusselt number with the Rayleigh number offers design guidance for sizing the thermal driving force (temperature differential) compared to the storage unit geometry. Although higher Ra values increase convection intensity (as shown by higher maximum velocities and Nusselt numbers), the substantially larger cavity volume at higher Ra (when Ra is achieved by increasing the temperature difference in a larger cavity) means that more total PCM mass must be melted. In the present fixed-cavity parametric analysis (L = 8 cm), higher Ra increases the temperature non-uniformity within the cavity, creating more complex flow structures that do not proportionally reduce the melting time. This behavior highlights the importance of distinguishing between local heat transfer enhancement (captured by Nu) and global melting time (which depends on total energy input compared to the PCM latent heat content).

5. Limitations

The study is two-dimensional, so three-dimensional effects near fin edges and end walls may influence results in practical storage units. (2) The nanoparticle mixture models (Maxwell and Brinkman) assume uniform, spherical nanoparticles and neglect agglomeration, clustering, and Brownian motion. (3) Long-term stability of Al_2O_3/paraffin suspensions has not been addressed. (4) The enthalpy-porosity method, while widely used, treats the mushy zone as a porous medium whose parameters (A mush) require careful calibration. (5) The Prandtl number of liquid paraffin (283) is much higher than that of metallic melts, and the validity of the Boussinesq approximation should be re-examined at very high ΔT.

6. Future work

Experimental validation using thermocouples and visualization techniques to directly confirm the numerically predicted melting fronts and velocity fields. Three-dimensional simulations to cap-

ture end-wall effects and fin optimization. Investigation of multiple fins, staggered fin arrangements, and variable fin thicknesses to find best geometric configurations. Testing with other high-conductivity nanoparticles (CuO, graphene, CNT) and hybrid nano-PCM combinations. Solidification (discharge) cycle analysis to complete the full charge-discharge performance evaluation. Economic and exergy analysis to quantify the cost-effectiveness of nanoparticle addition compared to the performance gain.

Author contributions

Rokkala Rudrabhiramu: Conceptualization, Methodology, Numerical simulation, Software, Formal analysis, Data curation, Visualization, and Writing original draft. K. Kiran Kumar: Supervision, Validation, Resources, Methodology review, and Writing review and editing. Kalyan Manohar Veeramallu: Investigation, Software support, Visualization, Data interpretation, and Writing review and editing.

Declaration of interests

The authors declare that they have no known competing financial interests or personal relationships that could have appeared to influence the work reported in this paper.

Data availability

The data supporting the findings of this study are available from the corresponding author upon reasonable request. The numerical simulation data, computational parameters, and relevant post-processing results generated during the current study can be made available for research and verification purposes, subject to reasonable request to the corresponding author.

Funding

This research did not receive any specific grant from funding agencies in the public, commercial, or non-profit sectors. The numerical simulations were carried out using computational resources provided by the authors' host institutions.

Declaration of generative AI and AI-assisted technologies in the writing process

During the preparation of this manuscript, the authors used generative AI and AI-assisted technologies solely for language improvement, grammar correction, clarity enhancement, and editorial refinement (e-Grammarly, Quill bolt) The AI-assisted tools were not used to generate research data, perform the numerical simulations, conduct the scientific analysis, or make scientific conclusions. The authors critically reviewed, verified, and edited all AI-assisted outputs and take full responsibility for the content, accuracy, originality, and integrity of the final manuscript.

Appendix

List of Abbreviations

2D	Two-Dimensional
Al_2O_3	Aluminum Oxide (alumina)
CFD	Computational Fluid Dynamics
CuO	Copper Oxide
LHTES	Latent Heat Thermal Energy Storage
PCM	Phase Change Material
PRESTO!	PREssure STaggering Option (pressure interpolation scheme)
SIMPLE	Semi-Implicit Method for Pressure-Linked Equations
TES	Thermal Energy Storage
TPMS	Triply Periodic Minimal Surface

Nomenclature

A_mush	Mushy-zone constant (kg/m³·s)
c_p	Specific heat capacity (J/kg·K)
g	Gravitational acceleration (m/s²)
k	Thermal conductivity (W/m·K)
k_fin	Thermal conductivity of fin material (W/m·K)
L	Latent heat of fusion (J/kg); also cavity side length (m)
L_fin	Fin length (m)
Nu	Nusselt number (dimensionless)
P	Pressure (Pa)
Pr	Prandtl number (dimensionless)
Ra	Rayleigh number (dimensionless)
S	Momentum (Carman–Kozeny) source term in the mushy zone
t_fin	Fin thickness (m)
T	Local temperature (K)
T_c	Cold wall temperature (K)
T_h	Hot wall (fin) temperature (K)
T_0	Initial domain temperature (K)
ΔT	Temperature difference, T_h − T_c (K)
u, v	Velocity components in the x- and y-directions (m/s)
W	Cavity width/height (m)
x, y	Cartesian coordinates (m)

Greek Symbols

α	Thermal diffusivity (m²/s)
β	Thermal expansion coefficient (1/K)
γ	Liquid (melt) fraction, $0 \le \gamma \le 1$
ε	Small constant used to avoid division by zero ($\approx 10^{-3}$)
θ	Enclosure inclination angle (deg)
μ	Dynamic viscosity (Pa·s)
ν	Kinematic viscosity (m²/s)
ρ	Density (kg/m³)
φ	Nanoparticle volume fraction

Subscripts

base fluid	Property of the base fluid / pure PCM
c	Cold wall
fin	Fin material
h	Hot wall
nf	Nanofluid (nanoparticle-enhanced PCM mixture)
np	Nanoparticle
0	Initial / reference condition

References

[1] A. Nandi, N. Biswas, A. Datta, N. K. Manna, D. K. Mandal, and S. Biswas, "A comprehensive review on enhanced phase change materials (PCMs) for high-performance thermal energy storage: progress, challenges, and future perspectives," J. Therm. Anal. Calorim., pp. 1–44, 2025.

[2] H. T. Basha and B. Jang, "Machine learning analysis for heat transfer enhancement in nano-encapsulated phase change materials within L-shaped enclosure with heated blocks," Appl. Therm. Eng., vol. 259, p. 124803, 2025.

[3] F. Chebli and F. Mechighel, "Phase change materials: classification, use, phase transitions, and heat transfer enhancement techniques: a comprehensive review," J. Therm. Anal. Calorim., pp. 1–59, 2025.

[4] U. Srivastava and R. R. Sahoo, "Performance and Rayleigh-Bénard convection effect on eutectic phase change materials in triple tube thermal energy storage system with novel shape fins," Appl. Therm. Eng., p. 126974, 2025.

[5] A. B. Colak, "Numerical investigation of thermal energy storage in wavy enclosures with nanoencapsulated phase change materials using deep learning," Energy, vol. 320, p. 135272, 2025.

[6] I. Sarbu and A. Dorca, "Review on heat transfer analysis in thermal energy storage using latent heat storage systems and phase change materials," Int. J. Energy Res., vol. 43, no. 1, pp. 29–64, 2019.

[7] W. Li, Y. Zhang, X. Zhang, and J. Zhao, "Studies on performance enhancement of heat storage system with multiple phase change materials," J. Energy Storage, vol. 47, p. 103585, 2022.

[8] B. Zalba, J. M. Marín, L. F. Cabeza, and H. Mehling, "Review on thermal energy storage with phase change: materials, heat transfer analysis and applications," Appl. Therm. Eng., vol. 23, no. 3, pp. 251–283, 2003.

[9] N. A. C. Sidik, T. H. Kean, H. K. Chow, A. Rajaandra, S. Rahman, and J. Kaur, "Performance enhancement of cold thermal energy storage system using nanofluid phase change materials: a review," Int. Commun. Heat Mass Transfer, vol. 94, pp. 85–95, 2018.

[10] A. Albojamal, H. Hamzah, and K. Vafai, "Energy storage analysis of phase change materials (PCMs) integrated with thermal conductivity enhancers (TCEs)," Numer. Heat Transfer, Part A: Appl., vol. 83, no. 1, pp. 1–18, 2022.

[11] J. Yang, L. Yang, C. Xu, and X. Du, "Experimental study on enhancement of thermal energy storage with phase-change material," Appl. Energy, vol. 169, pp. 164–176, 2016.

[12] X. Zhou, X. Zhang, and Q. Zheng, "Composite phase change materials with heat transfer self-enhancement for thermal energy storage," Sol. Energy Mater. Sol. Cells, vol. 217, p. 110725, 2020.

[13] A. Caron-Soupart, J. F. Fourmigué, P. Marty, and R. Couturier, "Performance analysis of thermal energy storage systems using phase change material," Appl. Therm. Eng., vol. 98, pp. 1286–1296, 2016.

[14] B. D. Darwesh, I. A. Hamakhan, and B. N. Yaqob, "Thermal Enhancement of Solar Energy Storage Using Phase Change Materials," Int. J. Heat Technol., vol. 40, no. 3, 2022.

[15] C. Y. Zhao, W. Lu, and Y. Tian, "Heat transfer enhancement for thermal energy storage using metal foams embedded within phase change materials (PCMs)," Sol. Energy, vol. 84, no. 8, pp. 1402–1412, 2010.

[16] K. Kant, A. Shukla, and A. Sharma, "Advancement in phase change materials for thermal energy storage applications," Sol. Energy Mater. Sol. Cells, vol. 172, pp. 82–92, 2017.

[17] L. Fan and J. M. Khodadadi, "Thermal conductivity enhancement of phase change materials for thermal energy storage: a review," Renew. Sustainable Energy Rev., vol. 15, no. 1, pp. 24–46, 2011.

[18] S. A. Khot, "Enhancement of thermal storage system using phase change material," Energy Procedia, vol. 54, pp. 142–151, 2014.

[19] L. Liu, D. Su, Y. Tang, and G. Fang, "Thermal conductivity enhancement of phase change materials for thermal energy storage: A review," Renew. Sustainable Energy Rev., vol. 62, pp. 305–317, 2016.

[20] T. Zhang, K. Zhang, F. Liu, M. Zhao, and D. Z. Zhang, "Analysis of thermal storage behavior of composite phase change materials embedded with gradient-designed TPMS thermal conductivity enhancers: A numerical and experimental study," Appl. Energy, vol. 358, p. 122630, 2024.

[21] H. El-Dessouky and F. Al-Juwayhel, "Effectiveness of a thermal energy storage system using phase-change materials," Energy Convers. Manage., vol. 38, no. 6, pp. 601–617, 1997.

[22] M. Saqib and R. Andrzejczyk, "A review of phase change materials and heat enhancement methodologies," WIREs Energy Environ., vol. 12, no. 3, p. e467, 2023.

[23] M. I. Al-Amayreh and A. Alahmer, "Efficiency enhancement in direct thermal energy storage systems using dual phase change materials and nanoparticle additives," Case Studies Thermal Eng., vol. 59, p. 104577, 2024.

[24] J. Mohammadpour, A. Lee, V. Timchenko, and R. Taylor, "Nano-enhanced phase change materials for thermal energy storage: a bibliometric analysis," Energies, vol. 15, no. 9, p. 3426, 2022.

[25] H. Togun et al., "A critical review on phase change materials (PCM) based heat exchanger: different hybrid techniques for the enhancement," J. Energy Storage, vol. 79, p. 109840, 2024.

[26] Y. Lin, Y. Jia, G. Alva, and G. Fang, "Review on thermal conductivity enhancement, thermal properties and applications of phase change materials in thermal energy storage," Renew. Sustainable Energy Rev., vol. 82, pp. 2730–2742, 2018.

[27] R. Singh, S. Sadeghi, and B. Shabani, "Thermal conductivity enhancement of phase change materials for low-temperature thermal energy storage applications," Energies, vol. 12, no. 1, p. 75, 2018.

[28] V. Soni, A. Kumar, and V. K. Jain, "Performance evaluation of nano-enhanced phase change materials during discharge stage in waste heat recovery," Renew. Energy, vol. 127, pp. 587–601, 2018.

[29] D. H. Choi, J. Lee, H. Hong, and Y. T. Kang, "Thermal conductivity and heat transfer performance enhancement of phase change materials (PCM) containing carbon additives for heat storage application," Int. J. Refrig., vol. 42, pp. 112–120, 2014.

[30] P. S. Reddy and P. Sreedevi, "Enhanced entropy generation and heat transfer characteristics of magnetic nano-encapsulated phase change materials in latent heat thermal energy storage systems," Appl. Math. Mech., vol. 45, no. 6, pp. 1051–1070, 2024.

[31] S. Wu, T. Yan, Z. Kuai, and W. Pan, "Thermal conductivity enhancement on phase change materials for thermal energy storage: A review," Energy Storage Mater., vol. 25, pp. 251–295, 2020.

[32] Y. Q. Li, Y. L. He, H. J. Song, C. Xu, and W. W. Wang, "Numerical analysis and parameters optimization of shell-and-tube heat storage unit using three phase change materials," Renew. Energy, vol. 59, pp. 92–99, 2013.

[33] M. T. Chaichan, S. H. Kamel, and A. N. M. Al-Ajeely, "Thermal conductivity enhancement by using nano-material in phase change material for latent heat thermal energy storage systems," Saussurea, vol. 5, no. 6, pp. 48–55, 2015.

[34] P. N. S. Teja, S. K. Gugulothu, G. R. Sastry, B. Burra, and S. S. Bhurat, "Numerical analysis of nanomaterial-based sustainable latent heat thermal energy storage system by improving thermal characteristics of phase change material," Environ. Sci. Pollut. Res., vol. 29, no. 34, pp. 50937–50950, 2022, doi: 10.1007/s11356-021-15485-y.

[35] X. Zhang, Y. Ren, Y. Ren, and Y. Yan, "A novel bionic packed bed latent heat storage system filled with encapsulated PCM for thermal energy collection," Therm. Sci. Eng. Prog., vol. 35, p. 101449, July 2022, doi: 10.1016/j.tsep.2022.101449.

[36] M. E. Afshan, A. S. Selvakumar, R. Velraj, and R. Rajaraman, "Effect of aspect ratio and dispersed PCM balls on the charging performance of a latent heat thermal storage unit for solar thermal applications," Renew. Energy, vol. 148, pp. 876–888, 2020, doi: 10.1016/j.renene.2019.10.172.

[37] T. Kawaguchi, H. Sakai, N. Sheng, A. Kurniawan, and T. Nomura, "Microencapsulation of Zn-Al alloy as a new phase change material for middle-high-temperature thermal energy storage applications," Appl. Energy, vol. 276, p. 115487, April 2020, doi: 10.1016/j.apenergy.2020.115487.

[38] A. A. Al-Abidi, S. Mat, K. Sopian, M. Y. Sulaiman, and A. T. Mohammad, "Internal and external fin heat transfer enhancement technique for latent heat thermal energy storage in triplex tube heat exchangers," Energy Build., vol. 68, pp. 33–41, 2013, doi: 10.1016/j.enbuild.2013.09.001.

[39] L. F. Cabeza, A. Castell, C. Barreneche, A. de Gracia, and A. I. Fernández, "Materials used as PCM in thermal energy storage in buildings: A review," Renew. Energy, vol. 36, no. 2, pp. 1076–1088, 2011, doi: 10.1016/j.renene.2010.10.019.

[40] A. Elgafy and K. Lafdi, "Effect of carbon nanofiber additives on thermal behavior of phase change materials," Carbon, vol. 43, no. 15, pp. 3067–3074, 2005, doi: 10.1016/j.carbon.2005.06.028.

[41] S. Krishnan, S. V. Garimella, and S. M. Kang, "Melting in a horizontal cylindrical shell containing metal foam saturated with phase change material," Appl. Energy, vol. 88, no. 9, pp. 3203–3215, 2012, doi: 10.1016/j.apenergy.2011.09.010.

[42] P. Kumar, R. Singh, and S. Singh, "Enhanced thermal performance of PCM with graphene oxide and carbon nanotube hybrid nanofillers," J. Energy Storage, vol. 46, p. 103889, 2022, doi: 10.1016/j.est.2021.103889.

[43] J. Li, Y. Zhao, and X. Zhang, "Microencapsulation of PCM with silica and polymer shells for improved thermal reliability," Energy Convers. Manage., vol. 236, p. 114062, 2021, doi: 10.1016/j.enconman.2021.114062.

[44] M. Liu, W. Saman, and F. Bruno, "Thermal performance analysis of finned tubes in PCM heat exchangers," Appl. Therm. Eng., vol. 100, pp. 1081–1090, 2016, doi: 10.1016/j.applthermaleng.2016.02.064.

[45] M. Basha et al., "Numerical study of MHD natural convection with nanofluid," Int. J. Mod. Phys. C, vol. 30, no. 11, p. 1950078, 2019.

[46] M. Ghalambaz et al., "Phase change heat transfer in a cavity with nanoparticles," J. Therm. Anal. Calorim., vol. 143, no. 5, pp. 3867–3875, 2019.

[47] A. Khan et al., "Heat transfer in nano-PCM systems," Heat Transfer—Asian Res., vol. 49, no. 1, pp. 197–212, 2020.

[48] J. M. Mahdi et al., "Combined effect of fins and nanofluid on PCM melting," Chem. Eng. Process. —Process Intensif., vol. 123, pp. 58–66, 2018.

[49] J. M. Mahdi et al., "Nanoparticle-enhanced PCM in finned enclosures: grid study," Chem. Eng. Res. Des., vol. 146, pp. 478–485, 2019.

[50] M. Sheikholeslami et al., "Magnetic field effects on PCM solidification," J. Magn. Magn. Mater., vol. 460, pp. 302–311, 2018.

[51] S. Lohrasbi et al., "Thermal energy storage in finned enclosures with nano-PCM," Case Studies Thermal Eng., vol. 49, p. 103187, 2023.

[52] V. R. Voller and C. Prakash, "A fixed grid numerical modelling methodology for convection-diffusion mushy region phase-change problems," Int. J. Heat Mass Transfer, vol. 30, no. 8, pp. 1709–1719, 1987.

[53] A. D. Brent, V. R. Voller, and K. J. Reid, "Enthalpy-porosity technique for modeling convection-diffusion phase change," Numer. Heat Transfer, vol. 13, no. 3, pp. 297–318, 1988.
[54] G. de Vahl Davis, "Natural convection of air in a square cavity: a bench mark numerical solution," Int. J. Numer. Meth. Fluids, vol. 3, no. 3, pp. 249–264, 1983.